Understanding Atmospheric Chemistry using Graph-Theory, Visualisation and Machine Learning.

Dan Ellis

March 2020

Veritatem inquirenti, semel in vita de omnibus, quantum fieri potest, esse dubitandu:
In order to seek truth, it is necessary once in the course of our life, to doubt, as far as possible, of all things.

- Descartes, Rene, *Principles of Philosophy*

Contents

Chapter 1

Computational Learning, Visualisation and Clustering:

Learning species structure using unsupervised machine learning.

"So, in the interests of survival, they trained themselves to be agreeing machines instead of thinking machines. All their minds had to do was to discover what other people were thinking, and then they thought that, too."

- Kurt Vonnegut, *Breakfast of Champions*

1.1 Introduction

Historical significance

The established process of trial and error has always underpinned our survival [Noble, 1957]. Babies are born to rely on a set of sensory reflexes and a framework for physical reasoning [Baillargeon and Carey, 2012], and with these, we develop methods to navigate the influence of change within a physical, and auditory space [Lynch, 2011]. This method of decision making is reflected in our adult lives with ideas and actions being limited in choice by our intuition and experience [Descartes and Lafleur, 1960]. In science, we apply a methodological framework consisting of a continuous assessment of scepticism, educated guessing (hypothesizing) and rigorous practical testing. Specialists accrue years of practical and theoretical knowledge within a narrow field and can identify areas of potential gain and futility. Yet even with all prior knowledge, the discovery of new and untested techniques involve the tortuous traipsing through a sea of uncertainty. Such a methods sometimes prove fruitful, through accidental discoveries of items such as x-rays, penicillin, etc. [Roberts, 1989]; finding novel applications for existing methods such as optical tweezers for chemistry or the abstract field of maths utilised by Einstein [REF], but more often than not end in the constant evolution of a pre-existing project with no clear result.

Theory and Simulation in Science

Until recently much of the experimentation possible was limited by resources, levels of knowledge available technology. With the increase of computation power, we have been able to not only increase our understanding but also run theoretical simulations to guide exploratory efforts with an impact on real-world applications [Oliveira et al., 2006; T. Leube et al., 2018; Morozov, 2016; Yu-ChenLo, 2018]. However, as our ability to record and produce data increases, the need for the scientific method diminishes [Anderson, 2008]. Here the application of ‘big data’ tools and algorithms can provide insights and correlations much more compelling than the predictive capabilities of constantly changing models - “Since all models are wrong the scientist cannot obtain a "correct" one by excessive elaboration” - Box [1976]. As our level of attainable technology increases, so does the complexity of the data collected. Modern data-sets tend to be large, complex and highly multivariate. Although this greatly improves the quality of science that may be extracted from them, the difficulty lies in trying to represent it in such a way that we may successfully access the reliability of the results. Since simple bar and line graphs are no longer applicable, one solution falls within a class of unsupervised machine learning techniques called dimensionality reduction (DR).

Chapter Aims

In **??** we looked at visual representation as a way of understanding complex systems. **??** showed that the chemical properties could be visually inferred from the node-link graph structure of a mechanism. Similarly, **??** and **??** located the presence of important species and clusters of like properties by applying mathematical algorithms to the graph network. As opposed to attempting to visualise complex data, this chapter looks at learning the structure of a chemical species and simplifying it into two dimensions. Here it is possible to extract key features of like-groups through the use of vector clustering, which unlike the graph clustering in **??** works by determining the density between points on a plane.

The chapter begins with the introduction of the chemical system, and the various methods for representing species structure within it (section 1.2). Next, we define the dimensionality reduction methods which shall be used to simplify the aforementioned inputs (**??**). This is followed by a brief overview of the visualisation methodology (**??**). Finally, all three sections are combined to produce a set of result and conclusions about the use of DR to identify species structure.

1.2 Species of the MCM and ways to represent them.

The master chemical system (as defined in all previous chapters), represents our foremost knowledge of gas-phase chemistry within the troposphere. It has been shown that due to its creation protocol (**??**), much of the information about a species structure is encoded within the reaction pathways it can take. This section explores the different methods of representing a species structure, intending to provide a machine built algorithm with the greatest amount of information about each species and its functionality. To do this a range of input types will be evaluated against several dimensionality reduction algorithms to isolate which chemical properties are most 'picked up'.

1.2.1 Input generation

The MCM provides species information in the form of a species 'smiles' (subsubsection 1.2.3.2) and the IUPAC InChi string [Heller et al., 2013]. Within this chapter, we use only the smiles string, which is either manually processed using regular expressions or with the aid of pythons RDKIT package [Landrum et al., 2019]. There are seven different methods for representing the chemistry, each of which are outlined below.

1.2.2 Manual Categorisation

Reactions within the MCM are determined by a set of rules (PROTOCOL SECTION). These are designed to mimic the process a chemist my discover new species and often rely on the bond availability and functionalisation of a species. Since the present functional groups are the benchmark of whether a DR algorithm has successfully separated species structure, it makes sense to run a unit test using the known functional groups of a species as the input.

To generate the functional groups the regular expressions in Table 1.1 are used[1] on the smiles strings (described in subsubsection 1.2.3.2) for each species. In extracting the functional groups we can plot the likeliness a species with a certain group is likely to have another using a chord diagram - Figure 1.1. Since most species are found to contain a multitude of functional groups, the separation of these into 'tidy' clustered groups seems unlikely.

PAN	C\\(=O\\)OON\\(=O\\)=O$|^\\[O-{0,1}\\]\\[N\\+{0,1}\\]\\(=O\\)OOC| O=N\\(=O\\)OOC\\(=O\\)|C\\(=O\\)OO\\[N\\+{0,1}\\]\\(=O\\)\\[O-{0,1}\\]
Carb. Acid	[^O](C\\(=O\\)O$|^OC\\(=O\\))
Ester	[\^O](C\(=O\)O\b|OC\(=O\))C
Ether	(\([\^O=]+\))*C(\([\^O=]+\))*O(\([\^O=]+\))*C(\([\^O=]+\))*
Per. Acid	c\\(=O\\)OO$|^OO\\(=O\\)C
Nitrate	O(NO2\b|NOO\b|N\(=O\)=O|\[N\+\](?:\[O-\]|\(=O\)){2})
Aldehyde	C=O$|^O=C
Ketone	C\(=O\)C
Alcohol	CO\\b|(?=^\\b)(?!^\\[)CO.|(?=^\\b)(?!^\\[)OC.|\\(O\\)|C\\)O(\\b|[^O]
Criegee	\[O-\]\[O\+\]
Alkoxy rad	\[[\/]{0,1}CH{0,1}\]|\b[\^O]\[O\.{0,1}\]
Peroxyacyl rad	\\ w\(=O\)O\[O\.{0,1}\]

Table 1.1: CHECKKKKKKK!!!!!!!!! A set of regular expressions that may be used to determine the number of occurrences of a functional group within a SMILES string.

[1] To see the structure of each functional group type, go to **??**.

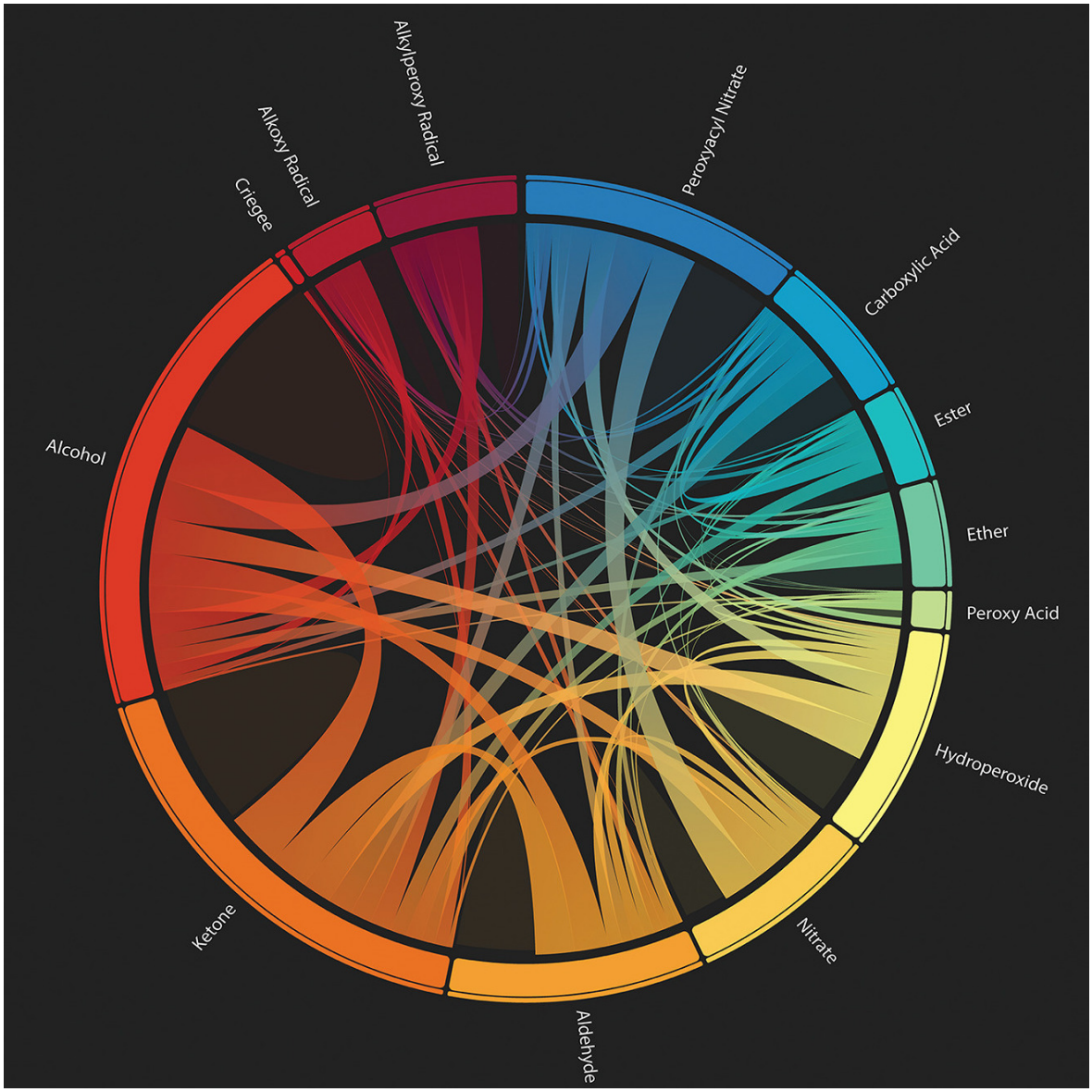

Figure 1.1: **The multifunctionality of the MCM.** A chord diagram showing the functionalisation of a species within the MCM. Arc sizes represent what percentage of all functional groups in the MCM mechanism a group contains. Translucent areas of no outwards links represent species with multiples of a certain functional group, of which Alcohols and Ketones have the most. Source: [Ellis, 2019]

1.2.3 Tokenization

As computer algorithms are unable to understand words or their meaning, we have to first categorise the data into groups. Tokenisation is the conversion of a string into characters and representing them with a numerical equivalent. In doing so a string of characters can be converted into a numerical vector, allowing for its representation in a latent vector space. Within our input selection, we have two sets of inputs we can convert. These are the species names, and their smiles string representation.

1.2.3.1 Species Names

In **??** it was shown that the dedicated species names for species in the CRI mechanism were often representative of their structural properties. This adage also applies for the MCM, where an intuitive naming convention has been selected. This is often derived as part of the construction protocol, where a species names reflect its own, or its precursor's structure (which it will have at least in-part inherited).

Although this is not the most robust method of defining the structure, it allows for an easy test of the algorithms, for which the user can quickly compare the human-readable output.

1.2.3.2 SMILES strings

Smiles ('Simplified Molecular-Input Line-Entry System') provide a human-readable representation of the molecular structure, [Weininger, 1988]. They provide a linear human-readable representation of the chemical structure within a molecule. This makes it easy for us to visually check the structure of a species without any additional work. Besides, their role in generating the molecular fingerprints in subsection 1.2.5 makes it a useful comparison to make when evaluating methods of structure representation.

Construction Methodology of SMILES strings

Smiles strings are constructed in three parts. We begin with a species backbone, then add break cycles and branches producing a smiles string. A visual description of this procedure is given below.

1. The smiles string is built by creating the longest possible chain to form a molecule backbone. Figure 1.2b
2. This may within itself contain aromatic rings denoted by the lowercase carbons and a number corresponding to the location of each break cycle. Figure 1.2c
3. Finally all the functional groups and branches attached to the main backbone are added. These are nested within the parenthesis to show that they are not part of the skeletal backbone. Figure 1.2d

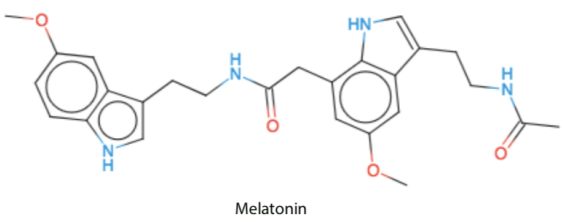

(a) Structure of Melatonin

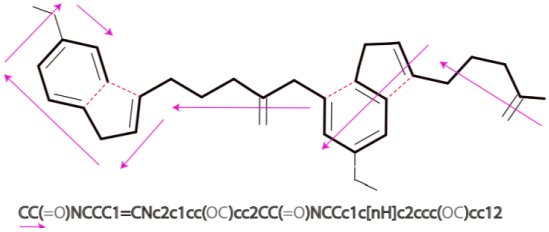

(b) Step 1 : Building the C chain backbone.

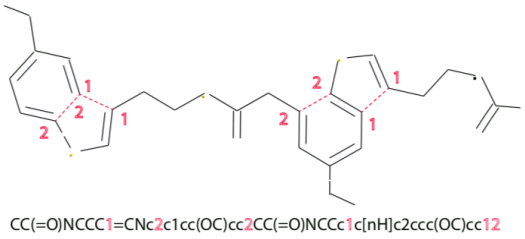

(c) Step 2 : Aromatic Rings

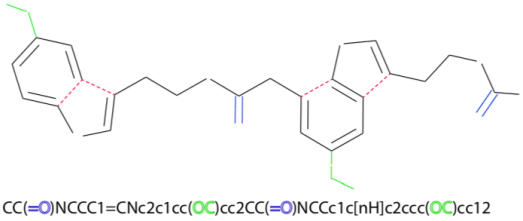

(d) Step 3 : Functional Groups

Figure 1.2: **Construction process of a smiles string.** The example compound is Melatonin. Although this does not exist within the atmosphere, it provides a clear example of the smiles string methodology. Figure 1.2a is made using smiles drawer: [Probst and Reymond, 2018]

1.2.4 Graph Inspired

?? - **??** have shown the role of graphs in revealing network properties and structure. Graphs in themselves can simplify relational data into two/three dimensions for visualisation and algorithmic clustering. Continuing this trend we can represent a species structure in the form of a graph (subsubsection 1.2.4.1), as well as converting the structure of a mechanism for dimensionality reduction (subsubsection 1.2.4.2)

1.2.4.1 The species graph (fingerprint)

The structure of a species has long represented using a graph-like layout, **??**. It, therefore, follows that other methods for representing the graph structure would also apply. One such method is the use of an adjacency (or relational) matrix to describe the relationships between atoms and bonds in a species. Such a methodology is already used in the construction of bond and z-matrixes, [**?**Parsons et al., 2005].

The construction of a structure matrix/graph begins with a chemical species. Here the relationships between atoms (Figure 1.3b) is converted into an adjacency matrix (Figure 1.3c). However since species have different numbers of each atom, a template allowing us to compare different graphs is required. To do this a maximum occurrence table (Figure 1.3a) is created. Here, for example, BCARY $C_{15}H_{24}$, a sesquiterpene contains the most carbon atoms of any species within the MCM. This universal matrix is now able to contain any possible combination of atoms in a species.

As machine learning algorithms only vectors as an input, it is possible to decompose the 37^2 element adjacency matrix into rows, which can then be joined together, Using this method we create a flat array (vector) of 259 elements (518 bytes) which can be used to represent our species.

Atom	**Max**
C	15
Cl	4
O	12
N	3
S	1
BR	2

(a)

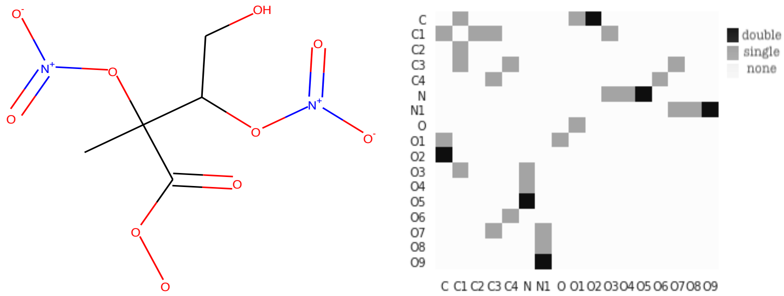

(b) (c)

Figure 1.3: **Constructing a graph from species structure.** (a) shows the maximum number of times an atom occurs for any single species in the MCM. (b) depicts the graph-like chemical structure of INB_1NBCO_3. This is a highly processed species stemming from Isoprene, and this makes for a good example of the bond matrix. Finally, a matrix representing the bonds in INB_1NBCO_3 is created from the maximum possible occurrence matrix from (a). For simplicity, empty row/column pairs have been removed to produce (c). This matrix will always be symmetrical as the bonds do not have a direction.

1.2.4.2 Node Embeddings (node2vec)

?? and **??** showed that the underlying structure of a chemistry mechanism graph contains information about the species and reactions within it. This is seen in Figure 1.4, where colour represents the ratio of potential oxidation of a species. Here as emitted species become progressively more processed, the number of bonds which may be oxidised diminishes (lighter colours near the centre) until they eventually form carbon dioxide and water.

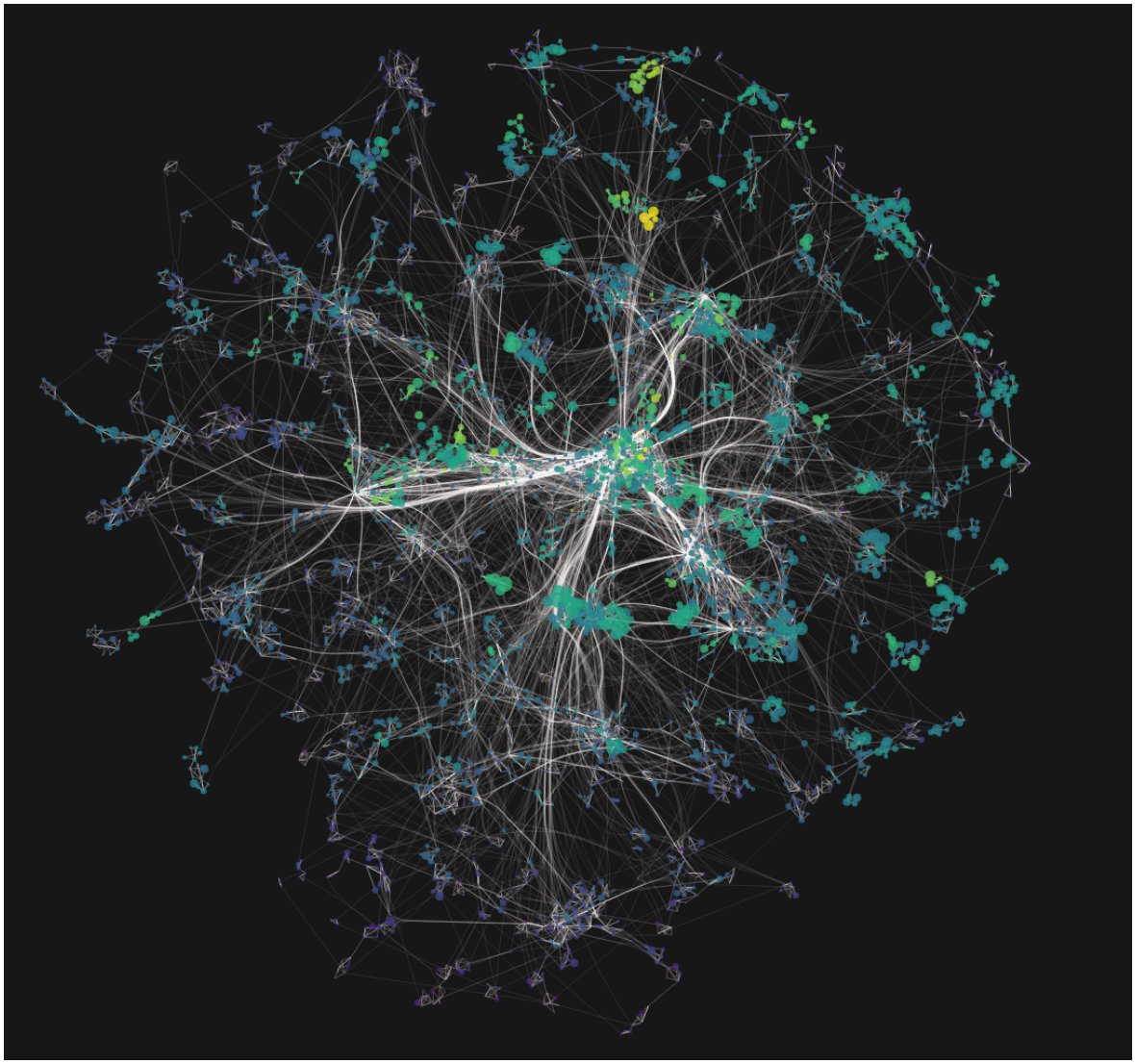

Figure 1.4: **The graph of an MCM subset representing the chemistry within Beijing.** Here colours show the increase of O−C ratio as species are oxidised (lighter). All emitted species ultimately tend towards carbon monoxide which is at the centre of the graph.

This type of structural information can be extracted through the use of a natural language processing package capable of transforming a graph into a vector - node2vec [Grover and Leskovec, 2019]. Since this may also be used for dimensionality reduction, it shall be described in the next section (subsection 1.3.6).

1.2.5 Molecular Fingerprints

In the field of chemical informatics, molecular fingerprints (or structural keys) are used to encode and query structural properties of species. Their binary representation makes them suitable for dimensionality reduction and the exploration of fo chemical space (a type of property space constructed using pre-determined properties and boundary conditions).

Here species properties are often split into structural and psyico-chemical groups - which has used such as the discovery of natural analogues (which circumvent problems such as intolerances in medicine [Spahn et al., 2017]). Although there exist many different types of molecular fingerprints, the two main ones that will be explored are molecular quantum numbers (MQN) and the molecular access system (MACCS).

1.2.5.1 Molecular Quantum Numbers (MQN)

In chemistry the shape, phase and electron occupancy of an atom may be described through the use of four quantum numbers: the n principle quantum number, I angular momentum quantum number, M_i magnetic quantum number and M_s spin quantum number. The rationalisation of elements based on their structure, and by consequence reactivity, has led to the most iconic tool of the modern-day chemist - the periodic table, where increasing atomic numbers follow the principal quantum number, [Wang and Schwarz, 2009]. In representing a molecule as a set of 42 quantum numbers, MQN fingerprints produce a multi-dimensional mapping of atom, bond, polarity and topology count [Nguyen et al., 2009].

1.2.5.2 Molecular ACCess System (MACCS)

MACCS keys are a 164[2] bit structural keys formulated through answering a series of structure-related questions. Developed by MDL Information Systems [, MDL], their main purpose lies in being a SMILES Arbitrary Target Specification (SMARTS) system for substructure searching. However, their distinct structure key format makes them highly suitable for similarity detection. In many cases, the optimised version of MACCS keys is cited ([Durant et al., 2002]), although most use cases exploit a variation of the undocumented 166bit keys. We use the implementation presented by [Landrum et al., 2019; rdkit, 2019] for all molecular fingerprints in this section.

1.3 Dimensionality Reduction Methods

In the last section we described a number of methods in which the chemical structure of a species could be incoded for direct comparison. However since each input is made up of a multitude of elements, it is still not a simple task determine the differences and similarity between all species in a mechanims. Dimensionality reduction is the process of reducing the number of random variables and only presentind a set of principal values, by mapping a high-dimensional space into a low-dimensional

[2]They are 166-bit keys, although there is no real agreement to what the 44th keys' purpose is, and therefore it is often omitted. Within RDKIT this is denoted by a ? [rdkit, 2019].

one, [Roweis and Saul, 2000]. This allows us to flatten a multivariate input into the two dimension required for a simple scatter plot.

In this section we begin by explaining the data preperation required for dimensionality reduction (**??**) before desribing the different possible methods of reducing the dimensions of a dataset.

1.3.1 Preperation of the data

Real-world data is rarely preformatted in such a way that it can be used directly within a computational model. Often values need to be cleaned and corrected to be fit for purpose. In the interest of completeness the two main methods of data adjustment for machine learning are outlined below. These are normalisation and standardisation.

Normalisation

In the data is without (dimensionless) or of a single unit, it is poissble to rescale the data between a range - most commonly 0,1. In doing so it is possible to interperate the importance of a value in contrast to the largest recorded value. This gives us a percentage scale spanning the range of the data. Such a range is useful in the definition of colourmaps and describing a values importance relative to the dataset. To rescale a dataset we shift the minimum value to zero, then divide by the new maximum of the dataset (Note this is equivalent to the range of the unshifted dataset.)

$$n(x_i) = \frac{x_i - \min_x}{\max_x - \min_x} \tag{1.1}$$

Standardisation

If the components we wish to compare are of differing units, or are expressed with a different scale, normalising them would not produce meaninful data. Instead it is possible to standardise the data by looking at each points deviation from the mean. This is done by dividing the variation of each point from the mean by the standard deviation of S and results in a value between $\{-1,1\}$, Equation 1.2. In statistics this is known as the 'z-score'[3]

$$z(x_i) = \frac{x_i - \mu_x}{S} \tag{1.2}$$

[3]Possibly because of the American spelling of standardi**Z**ation?

1.3.2 Principle Component Analysis

One of the most well known dimensionality reduction methods is the determination of the principal components through the use of Principal Component Analysis (PCA). PCA works on the assumption that components within a dataset are linear combinations of eachother. By simplifying these linear combinations, it is possible to identify the components which explain the most variability in a dataset - these are the principal components [F.R.S., 1901; Hotelling, 1933].

A simpler interpretation of this would be to adjust the direction of each axis of the data, such that its projection has the largest variability. In doing so it is possible to determine which components contribute the most to changes in the dataset. An example of this is seen in Figure 1.5 where the second component of the original data may be removed with little effect on the overall result of the data. Such methods have applications in compression and signal filtering [REF REF]

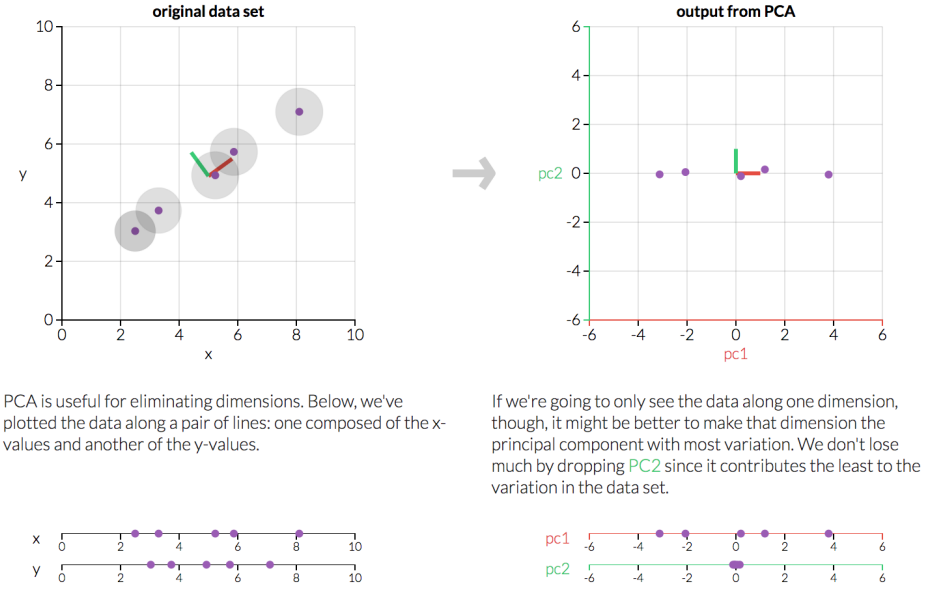

Figure 1.5: **Determining the Principal Compnent of a sample dataset.** It can be seen that in a change in axis to follow the first principal component (right), it is possible to explain most of the variation in the samle dataset (left). Source: [Powell, 2020]

1.3.2.1 Mathematical explanation of PCA

Note: *The basic statistics/mathematics required to understand this section is shown in* **??**. *Please read this if you are not familiar with any of the terms below.*

The mathematics behind PCA consists of first calculating the covariance matrix. This is an $n \times n$ matrix outlining how strongly each variable changes with every other. Using this we can calculate both the eigenvalues and eigenvectors of the matrix [4]. This may be done using a computational

[4]These need to be unit vectors, although most packages already do this out of the box.

package such as numpy or scipy [Oliphant, 2006; Jones et al., 01].

We can now sort the eigenvector columns by influence using their eigenvalues. This way a feature data-set can be produced by removing vectors of low influence. The final feature dataset can now be transposed and multiplied by the transpose of the original dataset. This produces an output dataset containing each principal component of the desired dimension.

1.3.3 t-Distributed Stochastic Neighbor Embedding (t-SNE)

t-SNE is an algorithm designed with visualisation in mind [Maaten and Hinton, 2008]. Rather than representing the data through a series of linear transformations, t-SNE uses local relationships to create a low-dimensional mapping, much in the same way as a fully connected force graph, **??**. This allows the ability to capture non-linear structures in the data which cannot be done through linear mapping methods (e.g. PCA).

The algorithm itself can be broken down into two parts[REF ttsne introduction paper]:

1. Create a probability distribution which dictates relationships between neighbouring points
2. Recreate a lower-dimensional space following the probability distribution established in 1.

The main reason t-SNE produces good results is that it can handle the 'crowding problem' very well.

Crowding Problem The crowding problem is a product of the 'curse of dimensionality. This is because, in high dimensional space, the surface of a sphere will grow much quicker than one in a lower dimension space. This means higher dimension spaces will have more points at a medium distance from a certain point, Figure 1.6. When we map our data into a lower dimension, data will try to gather at its medium distance, resulting in a more 'squashed', and thus crowded, output.

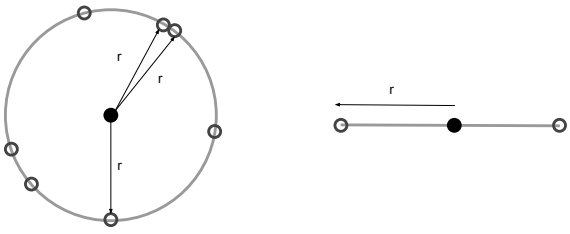

Figure 1.6: An example of how the curse of dimensionality affects the mapping of points a certian distance from eachother.

1.3.3.1 Mathematical explanation of t-SNE

In the original paper [Maaten and Hinton, 2008], the algorithm is described using the etymologic dissection of its name.

Step 1

First we begin with Stochastic Neigbour Embedding (SNE) - the distribution across neignbouring datapoints in our high dimension space. This is done by converting the high dimensional Euclidian distances between points into conditional probabilities representing their similarity:

$$p_{ij} = \frac{\exp(-\left\|x_i - x_j\right\|^2 / 2\sigma_i^2)}{\sum_{k \neq l} \exp(-\left\|x_k - x_l\right\|^2 / 2\sigma_i^2)} \tag{1.3}$$

Here $p_{i|j}$ is the conditional probability that x_i may pick x_j as a neigbour. This is proportional to the probability density of a Gaussian σ_i centered at x_i.

Perplexity Since we want the number of neighbours of each point to be similar in number and prevent a single point from having a disproportionate influence on the entire system we introduce a hyperparameter named *perplexity*. This works by ensuring that σ_i is small for points in densely populated areas and large for spare ones. This means that the perplexity of a system can be thought of as a scale of the number of neighbours considered for any one point. Generally, values between 5 and 50 are considered to give good results, with larger perplexities taking global features into account, and by consequence smaller ones, local features.

Step 2

Now a probability distribution describing the relationship between points has been formulated, we wish to express this as a low dimensional mapping of our inputs X in terms of our output dimensions Y. Naturally, we would want to make the low dimensional mapping represent a similar (Gaussian) distribution as in Step 1. However, it often causes issues presented by the 'overcrowding problem'section 1.3.3. This is because the gaussian has a 'short tail', and thus nearby points are likely to be pushed together. A solution to this is the student t-distribution which has a longer tail [5]:

$$q_{i|j} = \frac{(1 + \left\|y_i - y_j\right\|^2)^{-1}}{\sum_{k \neq l}(1 + \left\|y_k - y_l\right\|^2)^{-1}} \tag{1.4}$$

Note: *The definition and explination of the Student t-distribution is given in* **??**.

The optimisation of this equation can be achieved through the use of *gradient decent*[6] on the Kullback-Leibler divergence **??** between distributions p and q. Here the gradient is used to apply an attractive

[5]The distribution employed is a t-distribution with only one degree of freedom. This is identical to the Cauchy distribution

[6]**Gradient Decent** This is an optimisation algorithm used to minimise a function by iteratively moving in the direction of the steepest descent. This can be used to find local minima and is defined by the negative of the gradient.

and repulsive force on the items[7].

1.3.4 PCA vs t-SNE, a quick comparison.

PCA is one of the most used DR algorithms[ref list]. It is fast, simple and easy to use and very intuitive. The PCA algorithm works by creating a lower-dimensional embedding which best preserves the overall variance of the dataset. Clusters created from the algorithm are grouped in ways, such that they preserve the greatest variance.

The main drawback of PCA is that it is a linear projection. If our data happened to be in a 'swiss roll' (spiral) pattern, we would not be able to 'unroll' it. This is because PCA works by viewing the data from different perspectives, much like casting a shadow from various directions. With such an example, there is no one way we can do this that unfurls the spiral.

t-SNE, on the other hand, is a relatively new method [ref 06/08 paper]. Its greatest asset is that it is not limited by linear projections. Although more computationally intensive for large datasets, t-SNE produces visibly cleaner results. Unlike in PCA, t-SNE cannot be trained on additional data at a later point, however, the output clusters are more visually distinct (they have less overlap). Much like in a force graph, the output from t-SNE is scale-invariant. This means that whilst the location of clusters in a PCA reduced representation have an attributable quality, those produced by t-SNE will not necessarily contain the same information.

To test the differences between the two methods, a box model run representative of the chemistry within Beijing was used. The aim was to classify the diurnal profiles of each species concentration. To do this we standardised all the results and extracted the third day from a spun up model. These results were then fed into both the PCA and t-SNE algorithm. Figure 1.7 show the differences between the models. In Figure 1.7a we can see that the embedding is prone to overlap between species, with sample groupings (non-yellow species)[8] often being densely stacked on top of each other and indistinguishable from collections of species around them. Although only a slight improvement for the specified dataset, the t-SNE reduction allows the points to be better distributed, improving the definition of the group boundaries.

Its primary usage in machine learning is the updating of parameters (coefficients in linear regression and weight in neural networks).

[7] A positive gradient signifies attraction, whilst a negative one corresponds to repulsion.

[8] Species with similar profiles were grouped,Figure 1.7c

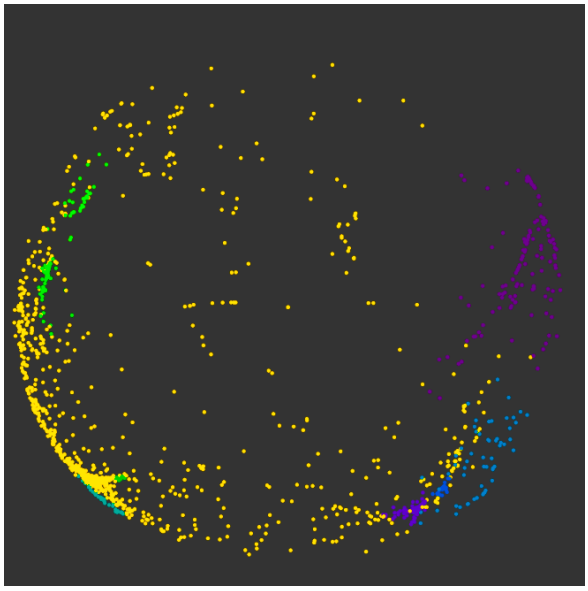

(a) PCA

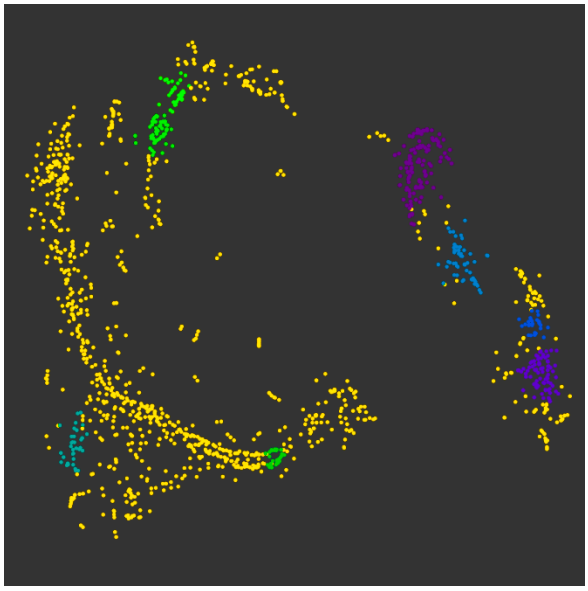

(b) t-SNE

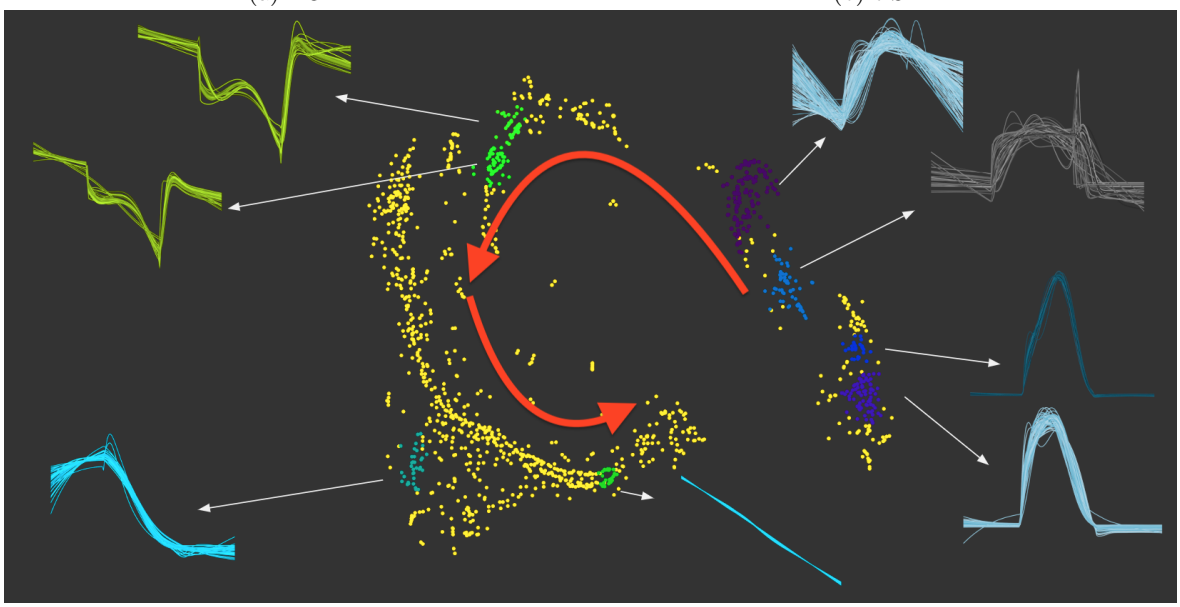

(c) t-SNE with cluster outlines.

Figure 1.7: Three simple graphs

1.3.5 The Auto-Encoder (AE)

Auto-encoders are a subclass of neural networks which are primarily used for dimensionality reduction. Rather than predicting a numerical output autoencoders focus on the construction and deconstruction of data through the use of an encoder and decoder pair. The encoder takes an n-dimensional input and applies a compression, reducing it to the number of dimensions in the bottleneck layer. This reduced dataset is then reconstructed within the decoder. Such a process not only allows for an easy understanding of the error of the reduced data but can also be used in the filtration of noisy or pixelated data [ref].

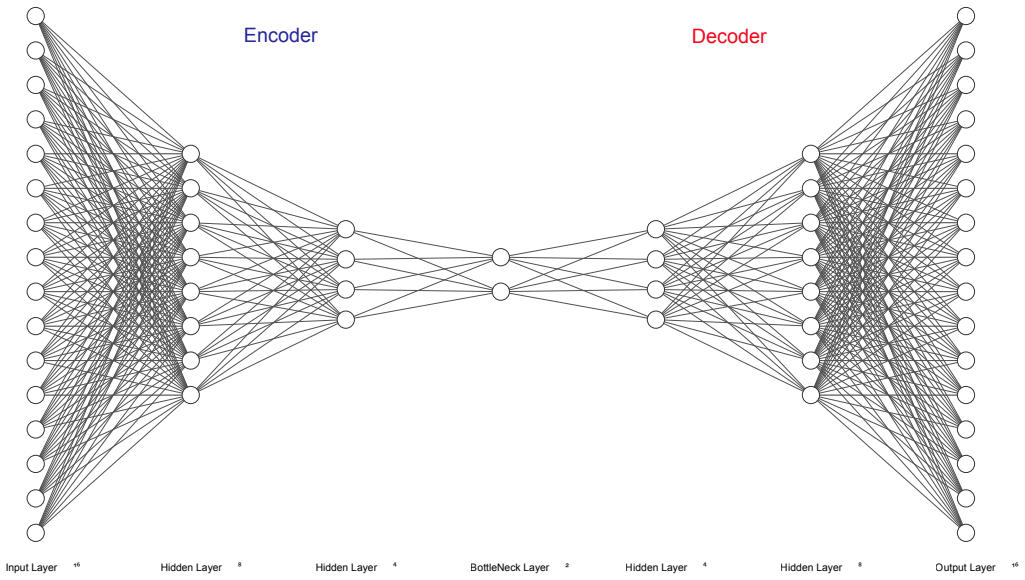

Figure 1.8: An example autoencoder structure which reduces a 16 dimentional input to 2. Draw with the aid of [Krizhevsky et al., 2012]

Usage in image reconstruction, signal processing or feeding large data into other models.

There are two features of an autoencoder that make it powerful. The first is the ability to sample your latent space using the decoder. This means we can establish features that correspond to gaps between our data points - which can have its application if the data used is sparse or incomplete. Next comes the inherent non-linearity of the model. As an autoencoder is just a neural network, the amount of information passed through each link between layers is governed by an activation function. Should this activation function be linear, the reduced dimension will be much akin to a PCA decomposition. However unlike PCA, in reducing the number of dimensions, we do not discard any data, but rather combine it - as per the nature of the links of the network. In trying to model/fit non-linearity, we have a range of activation functions to choose from. These are:

1.3.5.1 Demonstration of non-linear activation functions

To demonstrate the effect of these we take a sample isopleth of Methane and Ozone, reduce it to two dimensions, and then reconstruct it. Here we can see that some of the non-linearity of the original dataset has been lost when discarding the third principal component during PCA. Using a tanh activation function in an auto-encoder however, recreates much of the original properties of the data.

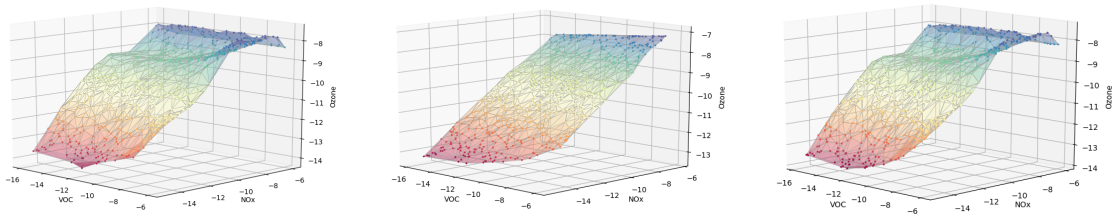

(a) Original (b) PCA (c) AE (Tanh)

Figure 1.9: Reducing the original dataset by 1 dimension and reconstructing it using different methods. Figure created using 300 simulations initialised with NOx (variable), Methane (variable) and Ozone (constant) using a Latin hypercube. The results are then plotted and converted into a surface using Delaunay triangulation.

1.3.6 Node2Vec

Node2Vec is an embedding algorithm designed to generate vector representations of the nodes in an *undirected* and *unweighted* network. This not only allows the input of graph derived relationships into other models, but can also be more computationally efficient, by circumventing the need for expensive composition, whilst producing better predictions on some network-related tasks compared to more classical methods, such as PCA [Grover and Leskovec, 2019].

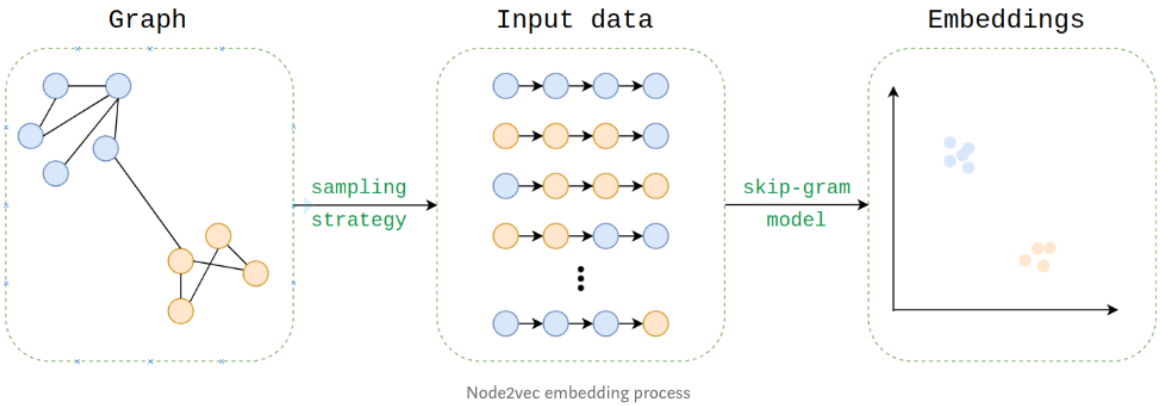

Figure 1.10: The process of converting a graph into a vector using Node2Vec. Source:[?]

The process of converting the graph structure (Figure 1.10) into a numerical vector node embedding starts by taking a series of 2^{nd} order random walks. These describe the neighbourhood of a node in the form of a set of random walk paths, much in the same way words are dependant on their neighbours within a sentence: Equation 1.5.

$$ISOPRENE \rightarrow OH \rightarrow TISOPA \rightarrow ISOPBO_2 \rightarrow TISOPA \rightarrow ... \tag{1.5}$$

1.3.6.1 Input / Sampling

The probability and path depend both on a set of arguments and a random seed provided to the model. The return and input parameters p, q determine how fast we explore the network and our probability to leave the neighbourhood, Figure 1.11. In a network, where the previous path is from t to v, we may calculate the probability of returning to t as $1/p$, going to a mutual node connected between t and v as 1, and viewing a new node as $1/q$. If $q > 1$ we have a high probability to end up at nodes close to t, and with $q < 1$ we are likely to explore other nodes. Additionally if we chose $p > \max q, 1$ we are less likely to return to an already visited node ($p < \min q, 1$ is likely to generate a backwards step). Since we wish to generate a 'local' view, but do not wish to return to t we select $q \geq 1$ and $p > q$ our parameters as $p = 2.0, q = 1.1$. In the case of a weighted graph (something that we are *not* exploring within this chapter) the resultant *alpha* value calculated is further multiplied by the edge weight.

To run the simulation we use the python 2 code provided by the original paper [Grover and Leskovec, 2019] with a set of 50000 random walks, each of length 9. The reasoning behind this is that we have a large graph, with a power-law like structure (within only a couple of steps we are connected to every other species within the network - that is if we do not include the inorganics, which in this case we are).

NOTE: This process takes over a week to compute, and then the binary file containing all walks in character form approaches 10 GB, for the complete MCM. ...in serial...

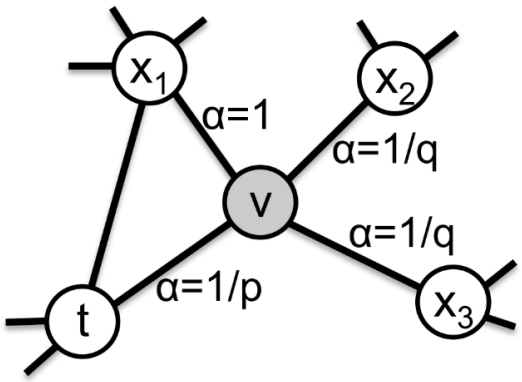

Figure 1.11: Calculation of the random walk path. Source:[Grover and Leskovec, 2019]

1.3.6.2 Word2Vec

Once we have constructed our random path 'sentences', we can make use of the well renowned word2vec algorithm developed by Google [**?**]. The word2vec algorithm is similar to an auto-encoder in many regards, but rather than learning word embeddings through reconstruction, it looks at the words (or

species in our case) which neighbour each other in our corpus. This form of representation has found many uses beyond the realm of natural language processing. Some of these are objects, people, code, tiles,genes and graphs [Lynch, 2011; ?; ?; ?; ?; ?].

https://skymind.ai/wiki/word2vec http://mccormickml.com/2016/04/19/word2vec-tutorial-the-skip-gram-model/

1.4 Results

1.4.1 CLuster distribution

Start with the visual comparison and compare it with the silhouette values.

Principle Component Analysis

DR	input	silhouette	groups
PCA	fngroups	0.9122	141
PCA	protocol	0.8761	149
PCA	node2vec	0.8569	3
PCA	maccs	0.6563	2
PCA	mqn	0.4041	8
PCA	smiles	0.3648	6
PCA	fingerprints	0.3529	6
PCA	spec	0.3364	6

Table 1.2: The inputs to the PCA dimensionality reduction algorithm sorted by the best obtained silhoette coefficient.

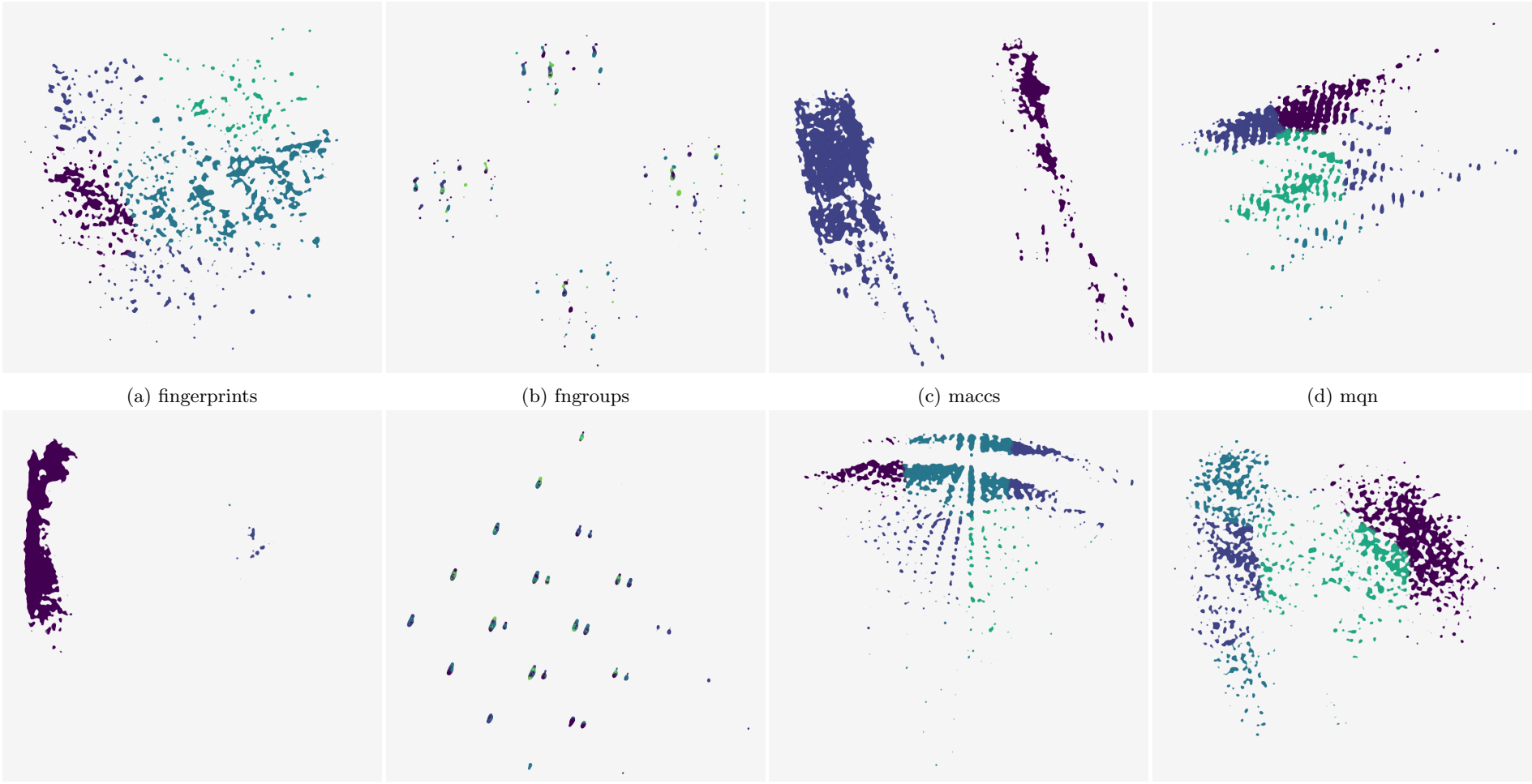

(a) fingerprints (b) fngroups (c) maccs (d) mqn

(e) node2vec (f) protocol (g) smiles (h) spec

Figure 1.12: **Comparing clusters for all inputs after a reduction to 2 dimsnsions using Principle Component analysis.** Each graphs has indergone several clustering algorithms under a range of parameters. The result with the best silhouette coefficient have been chosen. Colours follow the greedy 4 colour theorem and are there only to indicate contrast between cluster boundaries.

Auto Encoder Encoding

DR	input	silhouette	groups
AE	fngroups	0.9249	140
AE	protocol	0.8992	27
AE	smiles	0.6897	5
AE	mqn	0.6572	12
AE	maccs	0.6241	3
AE	node2vec	0.5476	5
AE	spec	0.4238	3
AE	fingerprints	0.3189	8

Table 1.3: The inputs to the AutoEncoder dimensionality reduction algorithm sorted by the best obtained silhoette coefficient.

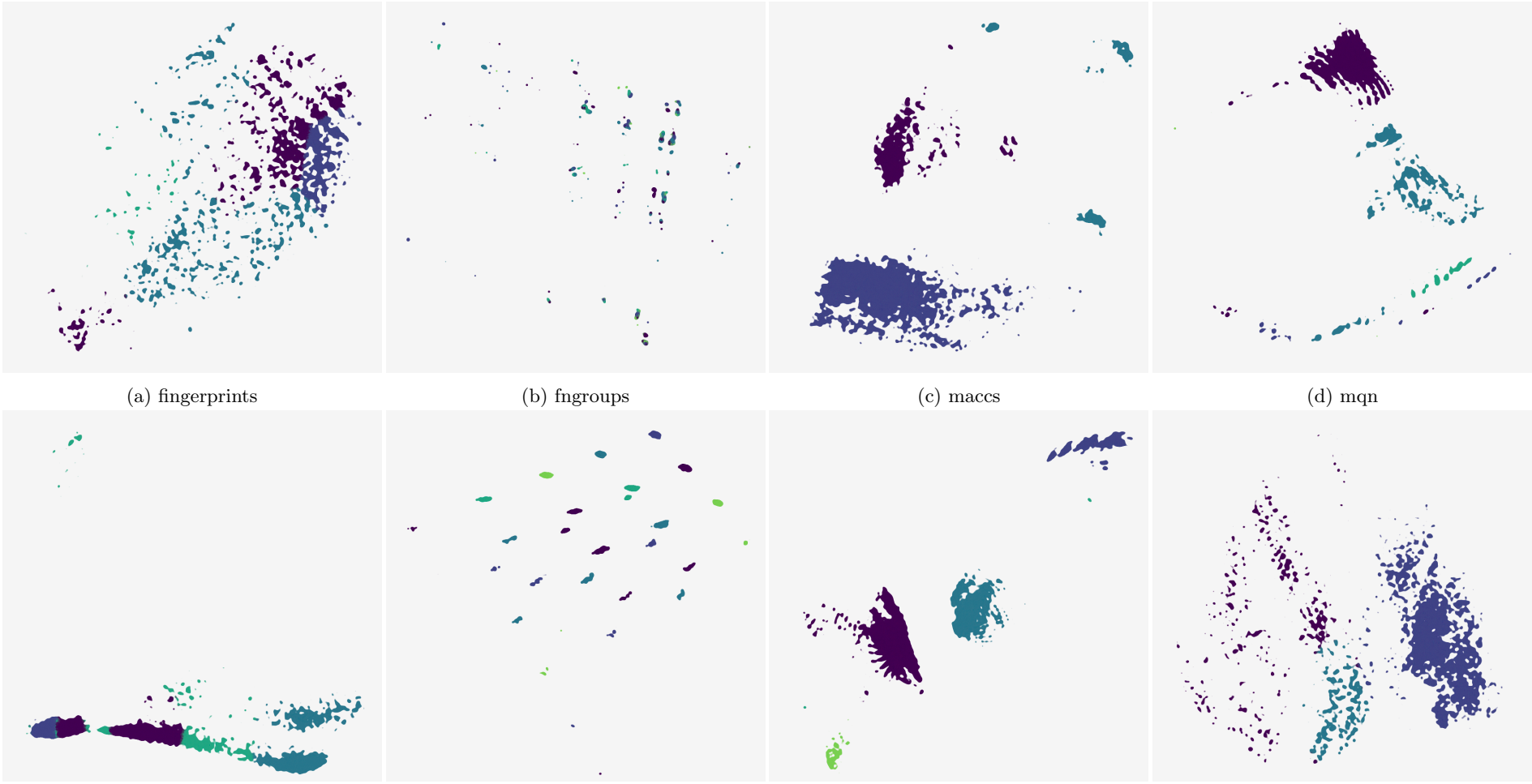

(a) fingerprints (b) fngroups (c) maccs (d) mqn

(e) node2vec (f) protocol (g) smiles (h) spec

Figure 1.13: **Comparing clusters for all inputs after a reduction to 2 dimsnsions using an AutoEncoder.** Each graphs has indergone several clustering algorithms under a range of parameters. The result with the best silhouette coefficient have been chosen. Colours follow the greedy 4 colour theorem and are there only to indicate contrast between cluster boundaries.

t-Distrubuted Stochastic Neighbor Embedding

DR	input	silhouette	groups
t-SNE	fngroups	0.7458	106
t-SNE	protocol	0.5688	51
t-SNE	smiles	0.4808	6
t-SNE	node2vec	0.4359	6
t-SNE	maccs	0.4295	3
t-SNE	spec	0.3781	35
t-SNE	mqn	0.3684	8
t-SNE	fingerprints	0.3539	6

Table 1.4: The inputs to the t-SNE dimensionality reduction algorithm sorted by the best obtained silhoette coefficient.

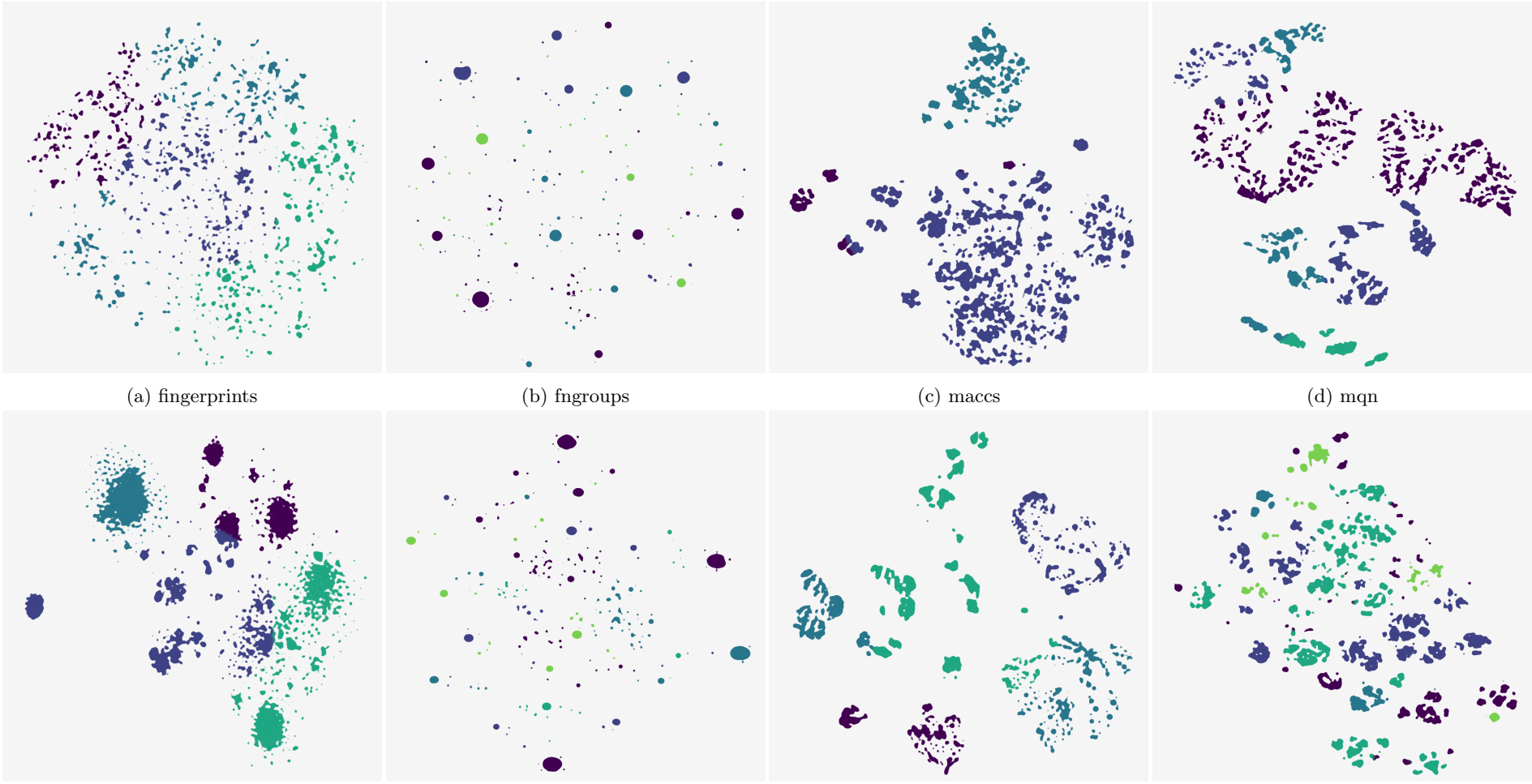

(a) fingerprints (b) fngroups (c) maccs (d) mqn

(e) node2vec (f) protocol (g) smiles (h) spec

Figure 1.14: **Comparing clusters for all inputs after a reduction to 2 dimsnsions using t-SNE.** Each graphs has indergone several clustering algorithms under a range of parameters. The result with the best silhouette coefficient have been chosen. Colours follow the greedy 4 colour theorem and are there only to indicate contrast between cluster boundaries.

Bibliography

Anderson, C. (2008). The End Of Theory: The Data Deluge Makes The Scientific Method Obsolete. *online*.

Baillargeon, R. and Carey, S. (2012). Core cognition and beyond: The acquisition of physical and numerical knowledge. *Early childhood development and later outcome*.

Box, G. E. P. (1976). Science And Statistics. *Journal of the American Statistical Association*, 71(356):791–799.

Descartes, R. and Lafleur, L. J. (1960). *Meditations On First Philosophy*. Bobbs-Merrill New York.

Durant, J. L., Leland, B. A., Henry, D. R., and Nourse, J. G. (2002). Reoptimization Of Mdl Keys For Use In Drug Discovery. *Journal of chemical information and computer sciences*, 42(6):1273–1280.

Ellis, D. (2019). Chemical Kinetic Interactions Cover Image. `https://s100.copyright.com/AppDispatchServlet?startPage=i&publisherName=Wiley&publication=kin&contentID=10.1002%2Fkin.21180&endPage=i&title=Cover+Image%2C+Volume+50%2C+Issue+6`. Accessed: 2019-6-6.

F.R.S., K. P. (1901). Liii. on lines and planes of closest fit to systems of points in space. *The London, Edinburgh, and Dublin Philosophical Magazine and Journal of Science*, 2(11):559–572.

Grover, A. and Leskovec, J. (2019). Node2vec: Scalable feature learning for networks. Accessed: 2019-10-21.

Heller, S., McNaught, A., Stein, S., Tchekhovskoi, D., and Pletnev, I. (2013). Inchi - The Worldwide Chemical Structure Identifier Standard. *Journal of cheminformatics*, 5(1):7.

Hotelling, H. (1933). Analysis of a complex of statistical variables into principal components. *Journal of Educational Psychology*, 24(6):417–441.

Jones, E., Oliphant, T., Peterson, P., et al. (2001–). Scipy: Open source scientific tools for Python. http://www.scipy.org/.

Krizhevsky, A., Sutskever, I., and Hinton, G. E. (2012). Imagenet Classification With Deep Convolutional Neural Networks. In Pereira, F., Burges, C. J. C., Bottou, L., and Weinberger, K. Q., editors, *Advances in Neural Information Processing Systems 25*, pages 1097–1105. Curran Associates, Inc.

Landrum, G., Tosco, P., Kelley, B., sriniker, gedeck, NadineSchneider, Vianello, R., Dalke, A., Cole, B., AlexanderSavelyev, Turk, S., Ric, Swain, M., Vaucher, A., N, D., Wójcikowski, M., Pahl, A., JP,

strets123, JLVarjo, O'Boyle, N., Berenger, F., Fuller, P., Jensen, J. H., Sforna, G., DoliathGavid, Cosgrove, D., Nowotka, M., Leswing, K., and van Santen, J. (2019). Rdkit 2019-03-2 (q1 2019) release.

Lynch, H. (2011). *Infant Places, Spaces And Objects: Exploring The Physical In Learning Environments For Infants Under Two*. PhD thesis.

Maaten, L. v. d. and Hinton, G. (2008). Visualizing Data Using T-Sne. *Journal of machine learning research: JMLR*, 9(Nov):2579–2605.

(MDL), M. I. S. (1984). Maccs-ii.

Morozov, A. (2016). Modelling biological evolution: Linking mathematical theories with empirical realities. *Journal of Theoretical Biology*, 405:1 – 4. Advances in Modelling Biological Evolution: Linking Mathematical Theories with Empirical Realities.

Nguyen, K. T., Blum, L. C., van Deursen, R., and Reymond, J.-L. (2009). Classification Of Organic Molecules By Molecular Quantum Numbers. *ChemMedChem*, 4(11):1803–1805.

Noble, C. E. (1957). Human Trial-And-Error Learning. *Psychological reports*, 3(2):377–398.

Oliphant, T. (2006). Guide to numpy.

Oliveira, B., Pereira, F., de AraÃºjo, R., and Ramos, M. (2006). The hydrogen bond strength: New proposals to evaluate the intermolecular interaction using dft calculations and the aim theory. *Chemical Physics Letters*, 427(1):181 – 184.

Parsons, J., Holmes, J. B., Rojas, J. M., Tsai, J., and Strauss, C. E. M. (2005). Practical Conversion From Torsion Space To Cartesian Space For In Silico Protein Synthesis. *Journal of computational chemistry*, 26(10):1063–1068.

Powell, V. (2020). Principal Component Analysis Explained Visually. `http://setosa.io/ev/principal-component-analysis/`. Accessed: 2020-2-25.

Probst, D. and Reymond, J.-L. (2018). Smilesdrawer: Parsing And Drawing Smiles-Encoded Molecular Structures Using Client-Side Javascript. *Journal of chemical information and modeling*, 58(1):1–7.

rdkit (2019). Rdkit.

Roberts, R. (1989). *Serendipity: Accidental Discoveries In Science*. Wiley Science Editions. Wiley.

Roweis, S. T. and Saul, L. K. (2000). Nonlinear dimensionality reduction by locally linear embedding. *Science*, 290(5500):2323–2326.

Spahn, V., Del Vecchio, G., Labuz, D., Rodriguez-Gaztelumendi, A., Massaly, N., Temp, J., Durmaz, V., Sabri, P., Reidelbach, M., Machelska, H., Weber, M., and Stein, C. (2017). A Nontoxic Pain Killer Designed By Modeling Of Pathological Receptor Conformations. *Science*, 355(6328):966–969.

T. Leube, B., Inglis, K., J. Carrington, E., Sharp, P., Shin, F., R. Neale, A., Manning, T., Pitcher, M., J. Hardwick, L., Dyer, M., Blanc, F., Claridge, J., and J. Rosseinsky, M. (2018). Lithium transport in li 4.4 m 0.4 m Â 0.6 s 4 (m = al 3+ , ga 3+ and m Â= ge 4+ , sn 4+): Combined crystallographic, conductivity, solid state nmr and computational studies. *Chemistry of Materials*, 30.

Wang, S.-G. and Schwarz, W. H. E. (2009). Icon Of Chemistry: The Periodic System Of Chemical Elements In The New Century. *Angewandte Chemie*, 48(19):3404–3415.

Weininger, D. (1988). Smiles, A Chemical Language And Information System. 1. Introduction To Methodology And Encoding Rules. *Journal of chemical information and computer sciences*, 28(1):31–36.

Yu-ChenLo (2018). Machine learning in chemoinformatics and drug discovery. *Drug Discovery Today*, 23(8):1538 – 1546.